Formation of gravastars

Daniel Jampolski

Institut für Theoretische Physik, Max-von-Laue-Strasse 1, 60438 Frankfurt, Germany

Luciano Rezzolla

Institut für Theoretische Physik, Max-von-Laue-Strasse 1,60438 Frankfurt, Germany
School of Mathematics, Trinity College, Dublin 2, Ireland and
CERN, Theoretical Physics Department, 1211 Geneva 23, Switzerland

Regular black holes and horizonless black hole mimickers offer mathematically consistent alternatives to address the challenges posed by standard black holes. However, the formation mechanism of these alternative objects is still largely unclear and constitutes a significant open problem since understanding their dynamical formation represents a first step to assess their existence. We here investigate, for the first time and without invoking higher-curvature corrections, the dynamical formation of a well-known horizonless black hole mimicker, namely, a gravastar. More specifically, starting from the collapse of a uniform dust sphere as in the case of the Oppenheimer-Snyder collapse, we demonstrate that, under fine-tuned conditions, a gravastar can form from the nucleation and expansion of a de Sitter region with initial zero size at the center of the collapsing sphere. Furthermore, the de Sitter expansion naturally slows down near the Schwarzschild radius, where it meets the collapsing dust surface and gives rise to a static equilibrium. Interestingly, we also find a maximum initial compactness of the collapsing star of $\mathcal{C} = 3/8$, above which the collapse to a black hole is inevitable.

Introduction. Black holes are important cornerstones of modern astrophysics and the end point of gravitational collapse [1, 2]. While their existence is perfectly compatible with gravitational-wave [3] and electromagnetic [4, 5] observations, some of the properties of black holes remain a source of concern and debate. Classical black holes, in fact, contain physical singularities where the predictability of general relativity breaks down. Additionally, they are shielded by an event horizon whose semiclassical evolution leads to problems with loss of information. To resolve these issues, alternative mathematical descriptions of black holes have gained significant attention over the last decades. These alternatives either remove the singularity while preserving the existence of an event horizon—as in the case of so-called "regular black holes"—or do not have either—as in the case of "black hole mimickers" (see, e.g., [6–19] for some regular black hole solutions or [20] for a recent review).

It is in this general context that the ingenious model of the gravitational vacuum condensate star, or gravastar, was first proposed [21, 22]. It comprises an interior of dark energy, described by the de Sitter solution and stabilized by a thin shell of ordinary matter. While the negative pressure of the dark energy seeks to expand the interior, gravity and a tangential pressure in the shell act as a belt preventing the expansion and leading to a static solution. Because a gravastar possesses neither a singularity nor an event horizon, and since its compactness can be brought arbitrarily close to that of a black hole, it has long been argued that it would be difficult to distinguish it from a black hole. When considering electromagnetic radiation as a route to distinguish the two objects, the debate is still ongoing (see, e.g., [23–25]), while it is clear that the different response to gravitational perturbations makes gravastars distinguishable from black holes [26, 27]. An aspect of gravastars that has so far not been addressed, mostly because of the challenges it poses, is their genesis from generic spherical distribution of matter (see however [28] for gravastar formation from the collapse of matter shells). We here present, for the first time, a model for the creation of a static gravastar following a gravitational collapse of a spherical cloud of matter.

Arrested Oppenheimer-Snyder Collapse. Our starting point for the construction of a gravastar formation model is the Oppenheimer-Snyder (OS) collapse [29]. This well-known solution, which physically describes the collapse of a homogeneous dust sphere to a black hole, is mathematically modeled by a Friedmann-Lemaitre-Robertson-Walker (FLRW) solution matched to an exterior Schwarzschild solution. In our case, since we eventually want to obtain a static gravastar, we need to add an expanding de Sitter region inside the collapsing FLRW spacetime, noting that the appearance of a de Sitter solution represents a common feature of most "bouncing" solutions in gravitational collapse (see, e.g., [11–13, 15]).

Thus, at any time in the evolution we separate spacetime into three different regions, I–III, with the line element for each region being given by

$$ds^2_{\rm I} = -dT^2 + a^2_{\rm I}(T)\left[dR^2/\left(1-k_{\rm I}R^2\right) + R^2 d\Omega^2\right] , \quad (1)$$

$$ds^2_{\rm II} = -d\tau^2 + a^2_{\rm II}(\tau)\left[d\rho^2/\left(1-k_{\rm II}\rho^2\right) + \rho^2 d\Omega^2\right] , \quad (2)$$

$$ds^2_{\rm III} = -\Phi(r)dt^2 + dr^2/\Phi(r) + r^2 d\Omega^2 . \quad (3)$$

Each region has its own set of coordinates, so that region I is the expanding FLRW de Sitter solution with (T, R) as a set of comoving coordinates for $0 \leq R < R_1$, while region II is the contracting FLRW dust solution with (τ, ρ) as a set of comoving coordinates for $\rho_1(\tau) < \rho < \rho_2$, and, finally, region III is a vacuum Schwarzschild solution with (t, r) as a set of Schwarzschild coordinates for $r > r_2(t)$.

Because the first two regions are described by FLRW solutions, they are characterized by two distinct scale factors $a_{\rm I}$ and $a_{\rm II}$, and by two spatial curvature constants $k_{\rm I} < 0$ (ex-

pansion from zero initial scale factor) and $k_{\rm II} > 0$ (collapse from initial static dust cloud), respectively. In the third region, instead, we have $\Phi(r) := 1 - 2M/r$ with M being the Schwarzschild mass, which is a constant of the spacetime. Without loss of generality, and because of the underlying spherical symmetry, all regions share the same spherical coordinates (θ, ϕ) with $d\Omega^2 := d\theta^2 + \sin^2\theta\, d\phi^2$. Clearly, R and ρ are not areal coordinates, while r is.

A few comments should be made before proceeding further. First, due to their comoving nature, $\rho_1 = \rho_1(\tau)$ and $r_2 = r_2(t)$, but also that $R_1 = $ const. and $\rho_2 = $ const. since they are the initial coordinate radii of the de Sitter bubble and of the dust sphere, respectively. Second, we assume that the energy density e and pressure p in the two FLRW spacetimes follow an equation of state $p_{\rm I} = -e_{\rm I}$ for the de Sitter region and $p_{\rm II} = 0$ for the collapsing dust region. Third, using the Friedmann equations it is possible to obtain that $e_{\rm I} = $ const. and $e_{\rm II} = \bar{e}_{\rm II}(\bar{a}_{\rm II}/a_{\rm II})^3$, where $\bar{e}_{\rm II} := e_{\rm II}(0)$ and $\bar{a}_{\rm II} := a_{\rm II}(0)$. Fourth, the expressions for the scale factors can be derived by solving the first of the Friedmann equations, obtaining $a_{\rm I}(T) = \sqrt{3|k_{\rm I}|/8\pi e_{\rm I}}\, \sinh\left(\sqrt{8\pi e_{\rm I}/3}\; T\right)$ for the de Sitter scale factor, and $a_{\rm II}(\eta) = \bar{a}_{\rm II}/2\, \left[1 + \cos\left(\sqrt{k_{\rm II}}\,\eta\right)\right]$ for the dust scale factor, where we have used the cycloid coordinate η with a coordinate transformation $d\eta = d\tau/a_{\rm II}$, so that $\tau(\eta) = \bar{a}_{\rm II}/2\, \left[\eta + \sqrt{1/k_{\rm II}}\sin\left(\sqrt{k_{\rm II}}\,\eta\right)\right]$. Fifth, it is useful to introduce the proper circumferential radii of the hypersurfaces dividing the three spacetimes, i.e., $\mathcal{R}_1 := \mathscr{C}_1/2\pi = a_{\rm I}(T) R_1$ and $\mathcal{R}_2 := \mathscr{C}_2/2\pi = a_{\rm II}(\eta)\rho_2$, where $\mathscr{C}_{1,2}$ are the proper (polar) circumferences of the hypersurfaces. Finally, we assume $a_{\rm I}(0) = 0$ and $\partial_\eta a_{\rm II}(0) = 0$, that is, the de Sitter bubble is initially of zero size and the dust collapses with zero initial velocity. We should note that while not uncommon in general relativity (e.g., point particles) zero-size objects represent the limitations of a classical theory. We here adopt it because it provides a mathematical simplification, but the initial zero-size de Sitter bubble could be replaced by a finite-size one without any impact on the dynamics we will describe. Obviously, if a quantum-gravitational description were possible, the zero-size de Sitter bubble would be naturally replaced by a Planck-size bubble.

Junction Conditions. Since we are patching together different solutions of the Einstein equations at the hypersurfaces between each region, we need to be careful in handling these separatrices. More specifically, we need to enforce junction conditions ensuring that the metric induced on the hypersurfaces is continuous across it [30]. Furthermore, it may be desirable that also the extrinsic curvature is continuous, although this is not a necessary condition for the patching to be valid. As in the OS collapse, the extrinsic curvature in our model is continuous at the dust hypersurface separating regions II and III. However, it is not continuous at the de Sitter hypersurface separating regions I and II as a result of the (infinite) radial-pressure gradient appearing when going from the expanding de Sitter bubble to the collapsing dust region. The loss of continuity is reflected by the appearance of a surface tension and of a surface energy density [31] on the de Sitter hypersurface.

While the junction conditions for the dust hypersurface can be found in textbooks (see, e.g., [32, 33]), which fix $\bar{e}_{\rm II}$, $r_2(t)$ and $t(\eta)$, the junction conditions for the de Sitter hypersurface need to be worked out. Imposing the continuity of the induced metric yields

$$\rho_1(T) = R_1 a_{\rm I}(T)/a_{\rm II}\left(\eta(T)\right), \tag{4}$$

and this gives the position of the de Sitter hypersurface as seen from an observer in the dust region. Similarly, the relation between the coordinate time in the collapsing dust region η and that in the expanding de Sitter region T is given by

$$\frac{d\eta}{dT} = \frac{R_1\rho_1\dot{a}_{\rm I}a'_{\rm II} \pm a_{\rm II}\sqrt{(k_{\rm II}\rho_1^2 - 1)\,(\rho_1^2/\rho_\star^2 - 1 - R_1^2\dot{a}_{\rm I}^2)}}{a_{\rm II}^2(\rho_1^2/\rho_\star^2 - 1)}, \tag{5}$$

where the choice of the minus sign corresponds to the positive time direction in η and where $\dot{a}_{\rm I} := \partial_T a_{\rm I}$ and $a'_{\rm II} := \partial_\eta a_{\rm II}$. Satisfying Eqs. (4)–(5), together with the junction conditions for the dust hypersurface, guarantees a valid patching of the different regions of the spacetime and, of course, that observers on either side on an hypersurface will measure the same values of $\mathcal{R}_1$ and $\mathcal{R}_2$.

An interesting feature of Eq. (5) is the divergence in the rate between the two times, which occurs when the de Sitter hypersurface reaches the so-called "critical radius" $\rho_\star(\eta)$ defined as

$$\rho_1(\eta) = \left[k_{\rm II} + \left(\frac{a'_{\rm II}}{a_{\rm II}}\right)^2\right]^{-1/2} = \rho_2\sqrt{\frac{r_2}{2M}} =: \rho_\star(\eta)\,. \tag{6}$$

When $\rho_1 \to \rho_\star$, the expansion of the de Sitter bubble stops, as seen from an observer in the dust region, that is

$$\frac{d\eta}{dT} \to \infty \;\;\Rightarrow\;\; \partial_\eta\, a_{\rm I}\left(T(\eta)\right) = \partial_T\, a_{\rm I}\left(\frac{d\eta}{dT}\right)^{-1} \to 0\,. \tag{7}$$

Results. Rather than seeking an initial solution that leads to a gravastar at the end of the collapse, it is far easier to start from a time when the collapse has terminated and the gravastar has just been formed, and integrate back Eq. (5) to find the set of conditions that lead to a successful configuration. Indeed, because tuning is required to ensure that the de Sitter surface comes to a rest when the gravastar is eventually produced, integrating back in time is essential to guarantee that the desired behavior is achieved.

Hence, our "initial" conditions at the "final" time $T_\star$ and $\eta_\star$ can be expressed in terms of the proper circumferential radii $\mathcal{R}_{1,2}$, i.e.,

$$\mathcal{R}_{1,\star} := a_{\rm I}(T_\star) R_1 = 2M\,, \tag{8}$$

$$\mathcal{R}_{2,\star} := a_{\rm II}(\eta_\star)\rho_2 = 2M + \epsilon\,, \tag{9}$$

where $\epsilon \ll 1$ in Eq. (9) is introduced because we want the outer shell to be just outside the Schwarzschild radius, but also to avoid numerical errors when approaching the divergence in Eq. (5). Two additional free parameters need to be

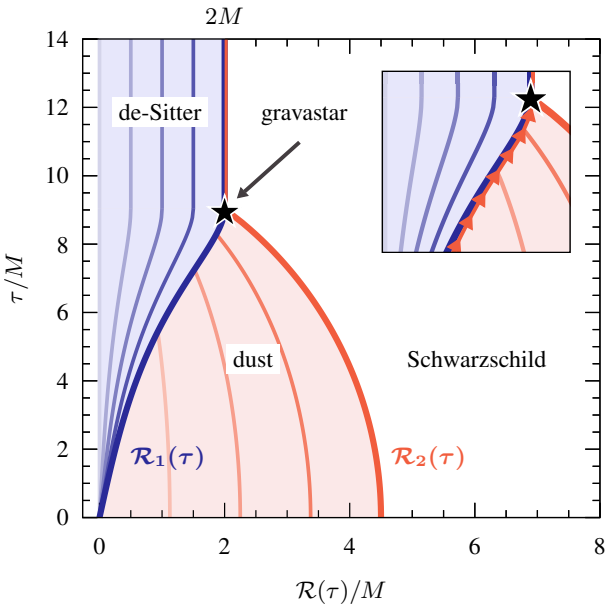

FIG. 1. Spacetime reporting the worldlines in proper time of the proper circumferential radii $\mathcal{R}_1$ (blue solid line) and $\mathcal{R}_2$ (red solid line) separating either the expanding de Sitter bubble (blue-shaded area) with the collapsing dust (red-shaded area), or the latter with the exterior Schwarzschild spacetime. Lines of the same color report worldlines at fractional values $1/4$, $1/2$, and $3/4$ of $\mathcal{R}_{1,2}$, respectively. Note the formation of a gravastar (black star symbol) when $\mathcal{R}_1 = \mathcal{R}_2$. The inset shows the dragging of the dust on the de Sitter surface due to the surface tension.

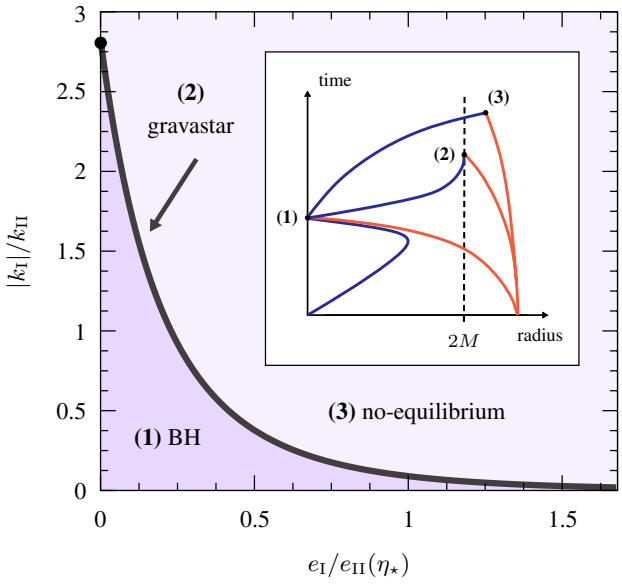

FIG. 2. Possible space of parameters for the collapse scenarios when expressed in terms of the energy density and spatial curvature of the de Sitter region. Shown with a black solid line are the set of $(e_{\rm I}, |k_{\rm I}|)$ values that lead to the successful creation of a gravastar [case (2)], so that configurations below the line lead to either the formation of a black hole [case (1)] or of a nonequilibrium configuration [case (3)]. The inset offers a schematic spacetime view of the three possible scenarios.

fixed for the integration of Eq. (5) and are given by the energy density and spatial curvature in region I, i.e., $e_{\rm I}$ and $k_{\rm I}$, respectively [34]. Furthermore, Eqs. (8) and (9) can be rearranged to specify the values of $T_\star$ and $\eta_\star$ (see End Matter for explicit expressions). After a choice for $e_{\rm I}$ and $k_{\rm I}$ is made, and requiring that $\rho_1 = \rho_\star = \rho_2$, we have all the initial conditions for the backward integration of Eq. (5), which we perform using an implicit Runge-Kutta scheme of fifth order.

Figure 1 offers, via a spacetime diagram, a representative example of the dynamical formation of a gravastar for $\bar{a}_{\rm II} = 1$, $\rho_2 = (9/2)M$, $|k_{\rm I}|/k_{\rm II} \simeq 2/3$, $e_{\rm I}/e_{\rm II}(\eta_\star) \simeq 1/3$, and $\epsilon \simeq 10^{-7}$. In particular, shown with a thick solid blue (red) line is the worldline of the circumferential radius $\mathcal{R}_1 = a_{\rm I}(T(\tau))R_1$ [$\mathcal{R}_2 = a_{\rm II}(\tau)\rho_2$] and with thinner lines the hypersurfaces at fractional values $1/4$, $1/2$, and $3/4$ of $\mathcal{R}_1$ ($\mathcal{R}_2$). Shown instead with a blue (red) area is the interior of the expanding de Sitter (collapsing dust) spacetime. Note that the expanding de Sitter bubble starts from a zero-size but nonzero initial velocity at $\tau = 0$ and that the two worldlines $\mathcal{R}_1$ and $\mathcal{R}_2$ reach $\mathcal{R}_{1,\star}$ and $\mathcal{R}_{2,\star}$ at $\tau = \tau_\star := \tau(\eta_\star)$, with $\mathcal{R}_1$ coming to a smooth stop (i.e., $d\mathcal{R}_1/d\tau \to 0$). Obviously, the inner part of the collapsing matter will interact with the edge of the expanding de Sitter bubble leading to a local increase in density, but not to a shock because of the collisionless nature of the dust. Furthermore, the presence of a surface tension at the de Sitter edge will prevent the "absorption" of the dust matter, which is pushed out by the expanding bubble (red arrows in the inset).

Producing a gravastar is only one of the three possible scenarios resulting from generic initial data [case (2) hereafter]. The other two possibilities have a final state with $\mathcal{R}_{1,\star} = \mathcal{R}_{2,\star} = 0$ [case (1) hereafter], or $\mathcal{R}_{1,\star} = \mathcal{R}_{2,\star} > 2M$ [case (3) hereafter]. These cases are summarized in Fig. 2, which reports with a solid black line the set of $(e_{\rm I}, |k_{\rm I}|)$ values leading to a successful gravastar formation. Values below the line (dark-shaded area) refer instead to a black hole formation, while values above the line (light-shaded area) refer to a configuration that may correspond (or not) to a stable but less-compact gravastar or to a nonequilibrium configuration. Also shown schematically in the inset are the three possible cases that we have illustrated above, where the initial position of the de Sitter bubble is chosen only for illustrative purposes.

Clearly, Fig. 2 shows that a gravastar is produced only for initial values of the energy density and spatial curvature lying on the separatrix between the different cases. In this sense, a point on the separatrix marks the only two values of $e_{\rm I}$ and $|k_{\rm I}|$ for which a gravastar can be produced, so that the separatrix cannot be an attractor of the solution. Rather, every point on the separatrix represents an "infinitely tuned" set of initial conditions leading to the formation of a gravastar. At the same time, because that point is also part of a one-parameter family of possible initial conditions, there are infinite sets of initial conditions leading to a gravastar. Stated differently, while the formation of a single gravastar is infinitely tuned, there are infinite different ways in which a gravastar can be produced. The properties of the space of parameters in Fig. 2 are

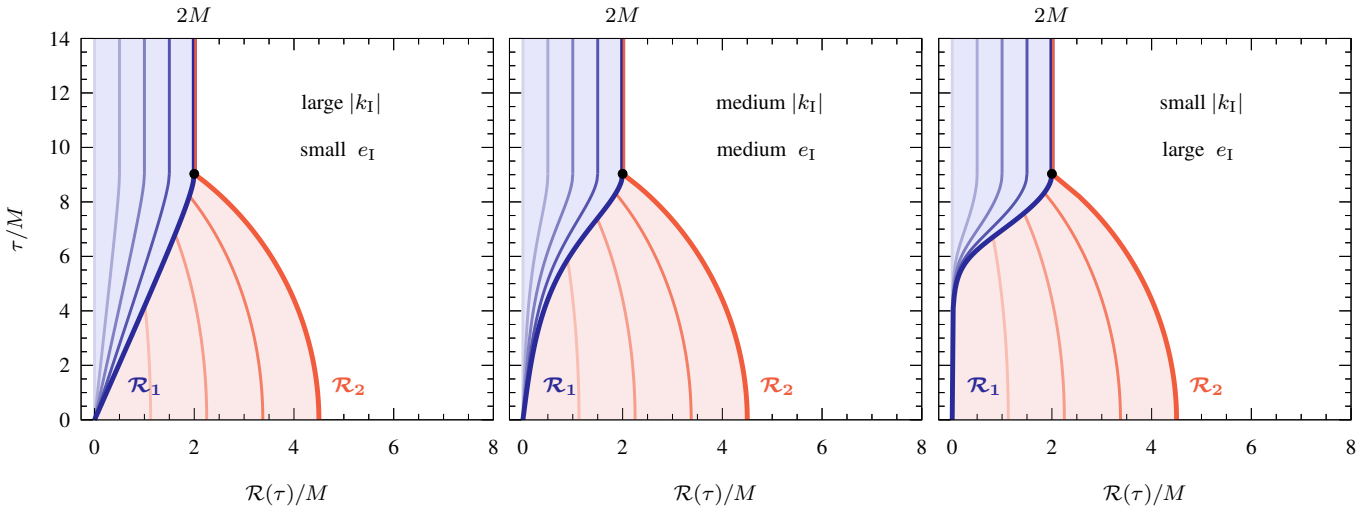

FIG. 3. The same as in Fig. 1 but for three sets of $(e_{\rm I}, |k_{\rm I}|)$ values referring either to a slow but constant de Sitter expansion [large $|k_{\rm I}|$, small $e_{\rm I} \to 0$; left panel], to an accelerated expansion [medium $|k_{\rm I}|$ and $e_{\rm I}/e_{\rm II}(\eta_\star) \simeq 2/3$; middle panel], or to an initially quiescent de Sitter bubble that experiences a late and very rapid expansion [small $|k_{\rm I}|$, large $e_{\rm I}/e_{\rm II}(\eta_\star) \simeq 10$; right panel].

still largely unknown and future work could explore whether a critical behavior is exhibited by solutions approaching the separatrix between cases (1) and (3), along which a gravastar formation is possible.

A series of remarks is worth making about Fig. 2. First, while the considerations made apply in general, the specific values reported refer to a specific initial radius of the dust sphere, i.e., $\bar{\mathcal{R}}_2 := \bar{a}_{\rm II}\rho_2 = (9/2)M$. Second, in general relativity case (1) necessarily leads to a black hole formation, but it can lead to a bouncing solution covered by an outer event horizon in alternative theories of gravity. Third, the energy density and the spatial curvature play a complementary role in the formation of the gravastar. As we discuss below, this has a direct impact on the speed at which the de Sitter bubble expands. Finally, while $|k_{\rm I}| \to 0$ when $e_{\rm I} \to \infty$, the opposite limit of $e_{\rm I} \to 0$ is particularly interesting and does not correspond to a divergent value of $k_{\rm I}$. Rather, it represents a Milne solution [35], that is, a flat Minkowski spacetime in hyperspherical coordinates or, alternatively, a FLRW solution with zero energy density, pressure, and cosmological constant (filled circle in Fig. 2).

To illustrate the complementary role played by the initial spatial curvature and energy density of the de Sitter region, we present in Fig. 3 three representative cases sharing the same $\bar{\mathcal{R}}_2$ but where we vary the values of $|k_{\rm I}|$ and $e_{\rm I}$. More specifically, the left panel refers to a situation with large $|k_{\rm I}|$ and small $e_{\rm I} \to 0$—note how the de Sitter edge expands with a nonzero but small initial velocity, which is kept constant for most of the evolution until it slows down just before meeting the surface of the collapsing dust sphere. The middle panel, instead, shows an evolution for intermediate values of $|k_{\rm I}|$ and $e_{\rm I}/e_{\rm II}(\eta_\star) \simeq 2/3$, that is very similar to that in Fig. 1 and for which we note that in this case the de Sitter edge has a smaller initial velocity but also that its evolution is accelerated in the later stages. Finally, the right panel of Fig. 3 shows the evolution for small $|k_{\rm I}|$ and large $e_{\rm I}/e_{\rm II}(\eta_\star) \simeq 10$, and exhibits a rather intriguing behavior whereby the de Sitter bubble does not expand but at very late times and it does so in a very rapid manner. This suggests that for $|k_{\rm I}| \to 0$ and $e_{\rm I} \to \infty$ it is possible to construct a gravastar where the collapse of matter takes place in a fully ordinary manner until when the stellar surface is very close to $\mathcal{R}_2 \gtrsim 2M$, at which point a de Sitter bubble is nucleated and expands extremely rapidly, meeting the dust surface at $\mathcal{R}_2 = 2M$.

Compactness Limit. A well-known result from the OS collapse is that the proper timescale for the formation of a black hole of mass M from a dust sphere of initial radius $\bar{\mathcal{R}}_2$ is $\tau = (\pi/2)[\bar{\mathcal{R}}_2^3/(2M)]^{1/2}$. For any compact object with $\bar{\mathcal{R}}_2 > 2M$, $\tau > \pi M$, so that dust clouds with compactness $\mathcal{C} := M/\bar{\mathcal{R}}_2 \lesssim 1/2$ are allowed. This logic no longer applies when producing a gravastar, since decreasing the initial dust radius forces the de Sitter expansion to occur faster, which can be accomplished by increasing $|k_{\rm I}|$, but only up to a limit. Stated differently, a causal threshold restricts the compactness of the initial dust sphere. To see this, we note that a photon emitted at $\eta = 0$ at the center of the dust sphere will take a time $\eta_\gamma = \sqrt{1/k_{\rm II}}\,\arcsin\left(\sqrt{k_{\rm II}}\rho_2\right)$ to reach the surface of the dust sphere at $\rho = \rho_2$. The compactness bound then follows from determining the initial dust radius that will be reached by such a photon before the dust surface reaches the Schwarzschild radius, i.e., $\eta_\gamma \leq \eta_\star$. This constraint sets the maximal compactness to be

$$\mathcal{C} = \frac{M}{\bar{\mathcal{R}}_2} \leq \frac{3}{8} = 0.375\,, \tag{10}$$

which is only slightly smaller than the Buchdahl limit of $\mathcal{C}_{\rm B} = 4/9 \simeq 0.444$ [36]. Interestingly, the limit $\mathcal{C} \to 3/8$ also requires that $|k_{\rm I}| \to \infty$ in order for the de Sitter bubble to be able to stop the collapse.

Conclusion. We have here provided a simple but comprehensive answer to a long-standing question: how is a gravastar formed? Starting from the OS collapse, we have embedded an expanding de Sitter bubble within the collapsing dust sphere. As a result, the evolving spacetime is split into three different regions patched together by junction conditions guaranteeing the continuity of the induced metric. In this way, it is possible to combine the relevant Friedmann equations for the two regions into a master differential equation that describes the three families of solutions reflecting the possible outcomes of the collapse process. In particular, we have shown that, depending on the initial conditions, the de Sitter expansion and dust collapse can either lead to a black hole, to a nonequilibrium configuration, or to a static gravastar. This latter outcome requires a fine-tuning of the initial spatial curvature and energy density in the de Sitter region, but there is an infinite family of initial conditions specified by a set of $(e_{\rm I}, |k_{\rm I}|)$ leading to the same static gravastar, although with different dynamics.

More specifically, large values of $|k_{\rm I}|$ and small values of $e_{\rm I}$ lead to a de Sitter bubble that expands with a nonzero but small initial velocity, which remains constant for most of the evolution before slowing down at gravastar formation. By contrast, small $|k_{\rm I}|$ and large $e_{\rm I}$ lead to a de Sitter bubble that expands only at very late times and it does so in a very rapid manner. This latter case suggests an appealing scenario in which the collapse of matter takes place in a fully ordinary manner until the stellar surface is very close to $2M$, at which point the de Sitter bubble can nucleate—e.g., as a result of quantum fluctuations, conformal anomaly [37–39], or instabilities in an anti-de Sitter spacetime [40]—and very rapidly stops the collapsing dust surface, forming a gravastar. Interestingly, because the whole process of gravastar formation cannot be superluminal, a maximum compactness of $\mathcal{C} \leq 3/8$ emerges for the dust sphere, above which the collapse cannot produce a gravastar but a black hole.

The dynamics presented here offers, for the first time, a rather straightforward example of how, remaining within general relativity and without invoking higher-curvature corrections, it is possible to avoid both singularity and black hole formation by employing the repulsive role of a de Sitter solution. At the same time, while our work shows that gravastar formation is possible, future studies will have to determine whether this scenario will continue to be possible under more realistic assumptions, such as the use of more realistic equations of state for the collapsing matter, the nucleation of de Sitter bubbles away from the center (potentially leading to a "nestar" solution [41]), or deviations from spherical symmetry that would lead to potential instabilities of the shell [42]. More importantly, additional studies will have to elucidate whether generic initial conditions in a gravitational collapse are more likely to lead to a gravastar or to a black hole.

Acknowledgements. It is a pleasure to thank A. Bonanno, F. Camilloni, F. Di Filippo, E. Mottola, and A. Murcia-Gil for useful discussions. Partial funding comes from the ERC Advanced Grant "JETSET: Launching, propagation and emission of relativistic jets from binary mergers and across mass scales" (Grant No. 884631). D.J. acknowledges support by the Hans-Böckler-Stiftung (German Academic Scholarship Foundation). L.R. acknowledges the Walter Greiner Gesellschaft zur Förderung der physikalischen Grundlagenforschung e.V. through the Carl W. Fueck Laureatus Chair.

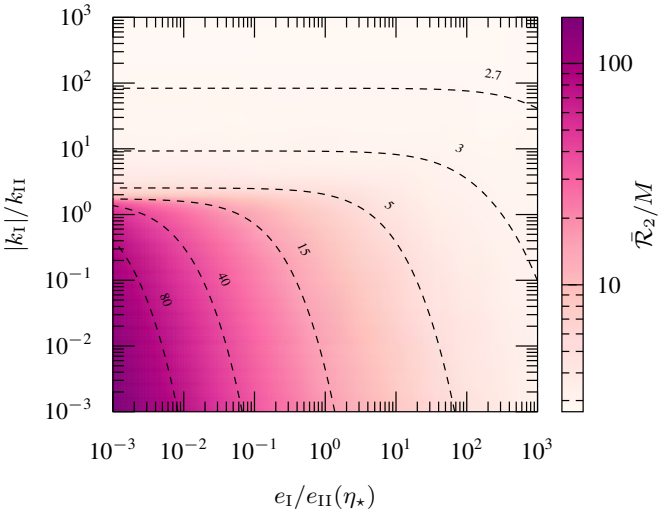

FIG. 4. The set of parameters $(e_{\rm I}, |k_{\rm I}|)$ leading to [case (2)] a gravastar formation, with different colors representing different initial dust radii $\bar{\mathcal{R}}_2$. Shown with dashed lines are contours corresponding to initial radii with $\bar{\mathcal{R}}_2/M = [2.7, 3, 5, 15, 40, 80]$.

Data Availability. The data that supports the findings of this article are not publicly available. The Data are available from the authors upon reasonable request.

Generalization to arbitrary dust configurations. While we have so far considered the formation of a gravastar from a specific dust configuration with $\bar{\mathcal{R}}_2/M = 9/2$, it is indeed possible to form a gravastar from an arbitrary initial radius so long as $\mathcal{C} \leq 3/8$. The parameter space in Fig. 2 can thus be extended to arbitrary initial radii $\bar{\mathcal{R}}_2/M \geq 8/3$, whilst only looking at case (2). Figure 4 reports with a color map the set of parameters $(e_{\rm I}, |k_{\rm I}|)$ leading to the formation of a gravastar, with different colors representing different initial radii $\bar{\mathcal{R}}_2$. Shown with dashed lines are the contours corresponding to initial radii with $\bar{\mathcal{R}}_2/M = [2.7, 3, 5, 15, 40, 80]$. Note that increasing $e_{\rm I}$ only slowly decreases the initial radii of the corresponding dust sphere, while a steep decrease happens when varying $k_{\rm I}$ for $|k_{\rm I}|/k_{\rm II} \in (1, 2)$.

Figure 5 depicts with different colors the collapse to a gravastar for initial radii $\bar{\mathcal{R}}_2/M \in (8/3, 8)$ and the corresponding motion of the hypersurfaces $\mathcal{R}_1(\tau)$ and $\mathcal{R}_2(\tau)$ for a fixed de Sitter energy density $e_{\rm I}/e_{\rm II}(\eta_\star) = 1$, which in turn determines the curvature constant $k_{\rm I}$. As mentioned in the main text, the timescale for the formation of a gravastar can

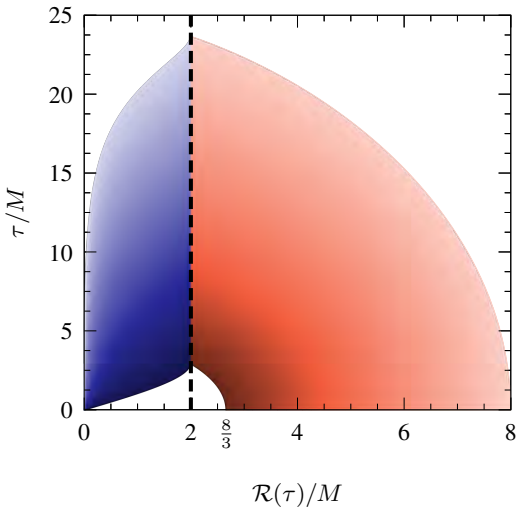

FIG. 5. Worldlines $\mathcal{R}_1(\tau)$ and $\mathcal{R}_2(\tau)$ for initial radii $\bar{\mathcal{R}}_2/M \in (8/3, 8)$ being represented by different colors for a fixed de Sitter energy density $e_{\rm I}/e_{\rm II}(\eta_\star) = 1$, which in turn determines the curvature constant $k_{\rm I}$.

be computed via (8)–(9), leading to

$$T_\star = \sqrt{3/8\pi e_{\rm I}}\,\text{arsinh}\left(2M\sqrt{8\pi e_{\rm I}}/\sqrt{3|k_{\rm I}|}R_1\right)\,, \tag{11}$$

$$\eta_\star = \sqrt{1/k_{\rm II}}\,\arccos\left([4M+2\epsilon]/\bar{\mathcal{R}}_2 - 1\right)\,, \tag{12}$$

which can be re-expressed in terms of $\tau_\star$.

Surface energy density and tension. Within the thin-shell description of two adjacent spacetimes, it is possible to define the surface stress-energy tensor

$$8\pi S_{\mu\nu} = A_{\mu\nu} - \frac{1}{2}A g_{\mu\nu}\,, \tag{13}$$

where $A_{\mu\nu}$ is the four-dimensional extrinsic curvature and $A := A^\mu_{\ \mu}$ is its trace (see, e.g., [30, 32, 33] for details). The discontinuity of the extrinsic curvature gives rise to a surface stress-energy three-tensor S_{ij} defined only on the de Sitter hypersurface

$$8\pi S_{ij} = \mp\left([K_{ij}] - [K]h_{ij}\right)\,, \tag{14}$$

where h_{ij} is the induced metric, K_{ij} is the extrinsic curvature, $K := K^i_{\ i}$ is its trace, and the square brackets measure a jump across the values $\psi^\pm$ of any quantity on either side of the hypersurface, i.e., $[\psi] := \psi^+ - \psi^-$. In our convention, "$-$" denotes region I (de Sitter) while "$+$" region II (dust). We should also remark that the surface stress-energy three-tensor S_{ij} can be seen as measuring the jump in the extrinsic curvature across the surface Σ separating the de Sitter and the dust region—hence as a purely geometrical quantity—or as measuring the jump in the stress-energy four-tensor across the same surface. In this latter case, it does not have a well-defined underlying microphysical description and hence a clear equation of state. It is therefore debatable whether such a virtual form of matter should obey an energy condition and whether a violation of an energy condition has any physical implication.

Choosing (T, θ, ϕ) as the coordinates on the de Sitter hypersurface, the nonzero components of the induced metric are given by

$$h^-_{TT} = -1\,, \tag{15}$$

$$h^-_{\theta\theta} = a_{\rm I}^2 R_1^2\,, \tag{16}$$

$$h^+_{TT} = -\dot\tau^2 + a_{\rm II}^2\dot\rho_1^2/x\,, \tag{17}$$

$$h^+_{\theta\theta} = a_{\rm II}^2\rho_1^2\,, \tag{18}$$

where x is an auxiliary variable defined as $x := 1 - k_{\rm II}\rho_1^2$, while the nonzero components of the extrinsic curvature tensor are given by

$$K^-_{\theta\theta} = a_{\rm I}R_1\sqrt{1+|k_{\rm I}|R_1^2}\,, \tag{19}$$

$$\begin{aligned} K^+_{TT} = -x^{-3/2}\big[&k_{\rm II}a_{\rm II}\rho_1\dot\rho_1^2\dot\tau - a_{\rm II}^2\partial_\tau a_{\rm II}\dot\rho_1^3 \\ &-x\left(a_{\rm II}\dot\rho_1\ddot\tau - a_{\rm II}\ddot\rho_1\dot\tau - 2\partial_\tau a_{\rm II}\dot\rho_1\dot\tau^2\right)\big]\,, \end{aligned} \tag{20}$$

$$K^+_{\theta\theta} = a_{\rm II}\rho_1 x^{-1/2}\left(x\dot\tau + a_{\rm II}\partial_\tau a_{\rm II}\rho_1\dot\rho_1\right)\,, \tag{21}$$

where a dot denotes a derivative with respect to T, so that $\dot\tau = \dot\eta a_{\rm II}$ and $\ddot\tau = \ddot\eta a_{\rm II} + \dot\eta^2 a'_{\rm II}$. Finally, due to spherical symmetry, $h^\pm_{\phi\phi} = h^\pm_{\theta\theta}\sin^2\theta$ and $K^\pm_{\phi\phi} = K^\pm_{\theta\theta}\sin^2\theta$.

The $S^T_{\ T}$ and $S^\theta_{\ \theta}$ components of the surface stress-energy tensor correspond, respectively, to the surface energy density and surface tension on the de Sitter hypersurface. While the surface tension is unavoidable, as it stabilizes the construction via a tangential pressure, the surface energy density can be chosen to be zero at the end of the collapse. We can see this by inspecting the quasilocal Misner-Sharp mass $dm/d\mathcal{R} = 4\pi\mathcal{R}^2 e$, and looking at the distributions of the different regions, being $M = M_{\rm I} + M_\Sigma + M_{\rm II}$, with $M_{\rm I} := (4\pi/3)e_{\rm I}\mathcal{R}_1^3$, and $M_{\rm II} := (4\pi/3)e_{\rm II}(\mathcal{R}_2^3 - \mathcal{R}_1^3)$. Since the energy density is homogeneous in all regions, the Misner-Sharp mass can easily be evaluated, and rearranged with respect to the surface mass

$$M_\Sigma = \frac{4\pi}{3}\mathcal{R}_1^3\left(e_{\rm II} - e_{\rm I}\right)\,, \tag{22}$$

which is proportional to the surface energy density $M_\Sigma \propto S^T_{\ T}$, so that if the surface energy density vanishes, the surface mass does so too.

The evolution of the surface mass M_Σ is shown in the left panel of Fig. 6, while that of the surface tension $S^\theta_{\ \theta}$ is reported in the right panel. The initial conditions for the dust parameters are the same as in Fig. 1, but the initial energy density in the de Sitter region is set to be $e_{\rm I}/e_{\rm II}(\eta_\star) = 1$, which leads to negative values during the collapse and to $M_\Sigma = 0$ at the end of the collapse. In this regard, we should note that what is relevant for an external observer is the total mass M of the system, which is positive and remains constant. Splitting such a mass in $M_{\rm I}$, $M_{\rm II}$, and M_Σ—which are derived quantities and do not have fundamental equations governing their dynamics—is done to recast these quantities in terms of an intuitive representation (e.g., the mass enclosed in a sphere of a

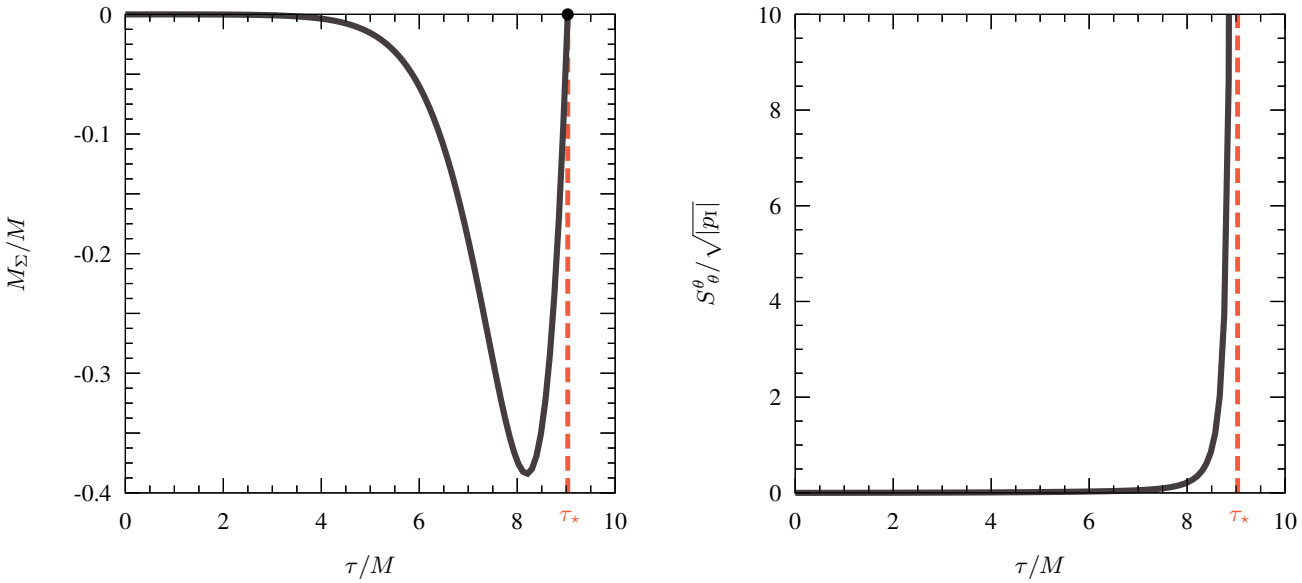

FIG. 6. Left panel: evolution of the surface mass M_Σ for the same dust parameters as in Fig. 1 but with a de Sitter energy density $e_{\rm I}/e_{\rm II}(\eta_\star) = 1$, leading to a vanishing surface energy density at the end of the collapse at $\tau_\star$. Right panel: evolution of the surface tension S^θ_θ, which builds up from zero, when the de Sitter expansion has not yet started, till divergence, when the dust gets compressed to zero thickness, as in a static gravastar.

radius $R_{\rm I}$ and $R_{\rm II}$), so that M_Σ is just the difference between the total mass M and the sum of $M_{\rm I}$ and $M_{\rm II}$, and can be negative. Indeed, M_Σ is not restricted to negative values and different initial conditions can lead to positive values throughout the gravastar formation process.

The fact that the surface mass becomes negative during the evolution can be explained in a number of different ways. First, to keep the total mass M constant while the mass of the de Sitter region $M_{\rm I}$ increases more rapidly than the decrease of the mass of the dust region $M_{\rm II}$. Alternatively, as a result of the choice of the initial (positive) energy density, which is $e_{\rm I} > e_{\rm II}$ essentially at all times and provides a negative contribution in Eq. (22). The behavior of the surface tension is instead simpler to understand and increases from an initial zero value, when the expansion of the de Sitter bubble has not started yet, diverging when the dust shell is compressed to zero thickness. This is in perfect agreement with what is expected for a static gravastar, where $S^\theta_\theta \to \infty$ in the limit of a zero-thickness shell, i.e., for $\epsilon \to 0$.

[1] R. Penrose, Gravitational collapse and space-time singularities, Phys. Rev. Lett. **14**, 57 (1965).

[2] R. Penrose and S. W. Hawking, The singularities of gravitational collapse and cosmology, Proc. Roy. Soc. Lond. A **314**, 529 (1970).

[3] B. P. Abbott *et al.* (Virgo, LIGO Scientific), Properties of the Binary Black Hole Merger GW150914, Phys. Rev. Lett. **116**, 241102 (2016), arXiv:1602.03840 [gr-qc].

[4] K. Akiyama and *et al.*, First M87 Event Horizon Telescope Results. I. The Shadow of the Supermassive Black Hole, Astrophys. J. Lett. **875**, L1 (2019).

[5] Event Horizon Telescope Collaboration, K. Akiyama, *et al.*, First Sagittarius A* Event Horizon Telescope Results. I. The Shadow of the Supermassive Black Hole in the Center of the Milky Way, Astrophys. J. Lett. **930**, L12 (2022).

[6] J. Bardeen, Non-singular general relativistic gravitational collapse, in *Proceedings of the 5th International Conference on Gravitation and the Theory of Relativity* (Tbilisi, USSR, 1968) p. 87.

[7] I. Dymnikova, Vacuum nonsingular black hole, General Relativity and Gravitation **24**, 235 (1992).

[8] S. A. Hayward, Formation and Evaporation of Nonsingular Black Holes, Phys. Rev. Lett. **96**, 031103 (2006), arXiv:gr-qc/0506126 [gr-qc].

[9] A. Simpson and M. Visser, Black-bounce to traversable wormhole, Journal of Cosmology and Astroparticle Physics **2019** (2), 042, arXiv:1812.07114 [gr-qc].

[10] R. Gambini, J. Olmedo, and J. Pullin, Spherically symmetric loop quantum gravity: analysis of improved dynamics, Classical and Quantum Gravity **37**, 205012 (2020), arXiv:2006.01513 [gr-qc].

[11] F. S. N. Lobo, M. E. Rodrigues, M. V. d. S. Silva, A. Simpson, and M. Visser, Novel black-bounce spacetimes: Wormholes, regularity, energy conditions, and causal structure, Phys. Rev. D **103**, 084052 (2021), arXiv:2009.12057 [gr-qc].

[12] A. Ashtekar, J. Olmedo, and P. Singh, Regular black holes from Loop Quantum Gravity, arXiv e-prints , arXiv:2301.01309 (2023), arXiv:2301.01309 [gr-qc].

[13] A. Masó-Ferrando, N. Sanchis-Gual, J. A. Font, and G. J. Olmo, Numerical evolutions of boson stars in Palatini f (R) gravity,

Phys. Rev. D **109**, 044042 (2024), arXiv:2309.14912 [gr-qc].
[14] A. Bonanno, D. Malafarina, and A. Panassiti, Dust Collapse in Asymptotic Safety: A Path to Regular Black Holes, Phys. Rev. Lett. **132**, 031401 (2024), arXiv:2308.10890 [gr-qc].
[15] P. Bueno, P. A. Cano, R. A. Hennigar, and Á. J. Murcia, Dynamical Formation of Regular Black Holes, Phys. Rev. Lett. **134**, 181401 (2025), arXiv:2412.02742 [gr-qc].
[16] R. Casadio, A. Kamenshchik, and J. Ovalle, From black hole mimickers to black holes, Phys. Rev. D **109**, 024042 (2024), arXiv:2401.03980 [gr-qc].
[17] H. Khodabakhshi, H. Lu, and F. Shojai, Gravitational Collapse: Generalizing Oppenheimer-Snyder and a Conjecture on Horizon Formation Time, arXiv e-prints , arXiv:2506.03702 (2025), arXiv:2506.03702 [gr-qc].
[18] R. Casadio, A. Kamenshchik, and J. Ovalle, Regular Schwarzschild black holes and cosmological models, Phys. Rev. D **111**, 064036 (2025), arXiv:2502.13627 [gr-qc].
[19] T. Harada, C.-M. Chen, and R. Mandal, Singularity resolution and regular black hole formation in gravitational collapse in asymptotically safe gravity, Phys. Rev. D **111**, 126017 (2025), arXiv:2502.16787 [gr-qc].
[20] R. Carballo-Rubio, F. Di Filippo, S. Liberati, M. Visser, J. Arrechea, C. Barceló, A. Bonanno, J. Borissova, V. Boyanov, V. Cardoso, F. D. Porro, A. Eichhorn, D. Jampolski, P. Martín-Moruno, J. Mazza, T. McMaken, A. Panassiti, P. Pani, A. Platania, L. Rezzolla, and V. Vellucci, Towards a non-singular paradigm of black hole physics, Journal of Cosmology and Astroparticle Physics **2025** (5), 003, arXiv:2501.05505 [gr-qc].
[21] P. O. Mazur and E. Mottola, Gravitational Condensate Stars: An Alternative to Black Holes, Universe **9**, 88 (2023), arXiv:gr-qc/0109035.
[22] E. Mottola, Gravitational vacuum condensate stars, in *Regular Black Holes: Towards a New Paradigm of Gravitational Collapse*, edited by C. Bambi (Springer Nature Singapore, Singapore, 2023) pp. 283–352, arXiv:2302.09690 [gr-qc].
[23] A. E. Broderick and R. Narayan, Where are all the gravastars? Limits upon the gravastar model from accreting black holes, Class. Quantum Grav. **24**, 659 (2007), arXiv:gr-qc/0701154.
[24] Event Horizon Telescope Collaboration, K. Akiyama, *et al.*, First Sagittarius A* Event Horizon Telescope Results. VI. Testing the Black Hole Metric, Astrophys. J. Lett. **930**, L17 (2022).
[25] R. Carballo-Rubio, F. D. Filippo, S. Liberati, and M. Visser, Constraints on thermalizing surfaces from infrared observations of supermassive black holes, Journal of Cosmology and Astroparticle Physics **2023** (11), 041, arXiv:2306.17480 [astro-ph.HE].
[26] C. B. M. H. Chirenti and L. Rezzolla, How to tell a gravastar from a black hole, Class. Quantum Grav. **24**, 4191 (2007), arXiv:0706.1513 [gr-qc].
[27] C. Chirenti and L. Rezzolla, Did GW150914 produce a rotating gravastar?, Phys. Rev. D **94**, 084016 (2016), arXiv:1602.08759 [gr-qc].
[28] K.-i. Nakao, C.-M. Yoo, and T. Harada, Gravastar formation: What can be the evidence of a black hole?, Phys. Rev. D **99**, 044027 (2019), arXiv:1809.00124 [gr-qc].
[29] J. R. Oppenheimer and H. Snyder, On continued gravitational contraction, Phys. Rev. D **56**, 455 (1939).
[30] W. Israel, Singular hypersurfaces and thin shells in general relativity, Nuovo Cimento B Serie **44**, 1 (1966).
[31] L. Rezzolla and J. C. Miller, Relativistic radiative transfer for spherical flows, Class. Quantum Grav. **11**, 1815 (1994), arXiv:astro-ph/9406055.
[32] E. Poisson, *A Relativist's Toolkit: The Mathematics of Black-Hole Mechanics* (Cambridge University Press, 2004).
[33] L. Rezzolla and O. Zanotti, *Relativistic Hydrodynamics* (Oxford University Press, 2013).
[34] We can always set $R_1 = 1$ since it is rescaled by the scale factor $a_{\rm I}$, set by our choice of $k_{\rm I}$.
[35] E. A. Milne, *Relativity, Gravitation and World-Structure*, International Series of Monographs on Physics (Clarendon Press (Oxford) / Oxford University Press (London), 1935).
[36] H. A. Buchdahl, General relativistic fluid spheres, Phys. Rev. **116**, 1027 (1959).
[37] E. Mottola and R. Vaulin, Macroscopic effects of the quantum trace anomaly, Phys. Rev. D **74**, 064004 (2006).
[38] E. Mottola, M. Chandra, G. M. Manca, and E. Sorkin, Quantum effects of the conformal anomaly in a 2D model of gravitational collapse, Journal of High Energy Physics **2023**, 223 (2023), arXiv:2303.15397 [gr-qc].
[39] E. Mottola, Gravitational vacuum condensate stars in the effective theory of gravity, Phys. Rev. D **111**, 104018 (2025), arXiv:2502.02519 [gr-qc].
[40] A. Biasi, O. Evnin, and S. Sypsas, de Sitter Bubbles from Anti-de Sitter Fluctuations, Phys. Rev. Lett. **129**, 251104 (2022), arXiv:2209.06835 [gr-qc].
[41] D. Jampolski and L. Rezzolla, Nested solutions of gravitational condensate stars, Classical and Quantum Gravity **41**, 065014 (2024), arXiv:2310.13946 [gr-qc].
[42] H. Yang, B. Bonga, and Z. Pan, Dynamical Instability of Self-Gravitating Membranes, Phys. Rev. Lett. **130**, 011402 (2023), arXiv:2207.13754 [gr-qc].